

HIGGS RARE AND EXOTIC DECAYS

LJILJANA MORVAJ^{a b}
*CERN, Esplanade des Particules 1,
 1217 Meyrin, Switzerland*



Several recent searches for exotic and rare decays of the Standard Model Higgs boson with the ATLAS and CMS detectors are presented. The searches are performed on $\sqrt{s}=13$ TeV proton-proton collisions data collected at the LHC between 2015 and 2018. The topics covered include searches for the Higgs boson decays into two pseudoscalars, $H \rightarrow aa$, in three different final states, $2b2\mu$, $4b$ and $2\mu2\tau$, search for lepton-flavour violating Higgs decays, $H \rightarrow \mu\tau/e\tau$, and search for a rare $H \rightarrow \ell\ell\gamma$ decay. ATLAS presents evidence for the $H \rightarrow \ell\ell\gamma$ rare decay, amounting to an observed significance of 3.2σ .

1 Introduction

Rare and exotic Higgs boson decays searches provide important tests of the Standard Model (SM) and could lead to a discovery of new physics. Current fits to the SM Higgs couplings constrain the branching fractions of the Higgs boson to undetected, $B(H \rightarrow \text{undetected})$, and invisible, $B(H \rightarrow \text{invisible})$, final states to be less than 19% and 9%, respectively¹. This leaves a lot of space for new physics in the Higgs boson decays. This talk presents several recent results delivered by the ATLAS² and CMS³ collaborations using 13 TeV proton-proton collision data collected at the LHC. Three types of searches are covered: Higgs decays into beyond-the-SM (BSM) states ($H \rightarrow aa \rightarrow 2b2\mu/4b/2\mu2\tau$), lepton flavor violating Higgs decays ($H \rightarrow \mu\tau/e\tau$) and rare Higgs decays ($H \rightarrow \ell\ell\gamma$).

2 Higgs decays to pseudoscalars

Light bosons appear in many well-motivated extensions of the Standard Model. For example, they could be mediators between the SM and some hidden sector that does not interact through the weak, strong or electromagnetic forces⁴. Searches for light pseudoscalars in Higgs boson decays are often interpreted in Two-Higgs-Doublets plus a Singlet (2HDM+S) set of models⁴.

^aOn behalf of the ATLAS and CMS Collaborations

^bCopyright 2021 CERN for the benefit of the ATLAS and CMS Collaborations. Reproduction of this article or parts of it is allowed as specified in the CC-BY-4.0 license.

The pseudoscalar component of the singlet field (a) acquires Yukawa-like couplings to SM particles through mixing with Higgs bosons. This implies that the largest branching fractions of the a -boson will generally be to b -quarks and τ -leptons. For a -masses (m_a) that are significantly lower than the SM Higgs boson mass, the a -boson is boosted and its decay products are collimated. Merging of b -jets and hadronically decaying τ -leptons into one reconstructed object starts below roughly $m_a=25$ GeV. ATLAS and CMS have developed dedicated reconstruction and identification techniques to address such boosted final states.

2.1 $H \rightarrow aa \rightarrow 2b2\mu$

The final state with two b -jets and two muons⁵ provides a good balance between the typically large decay fraction of $a \rightarrow bb$ and a clean signature of a narrow dimuon resonance from the $a \rightarrow \mu\mu$ side. This feature of the decays is further exploited in a kinematic-likelihood (KL) fit. In the fit, the di- b -jet mass (m_{bb}) is constrained, within its resolution, to the dimuon mass ($m_{\mu\mu}$) measured with approximately ten times better resolution. The output of the KL fit is the maximum likelihood score, which can be used to select events satisfying the $m_{bb} \sim m_{\mu\mu}$ hypothesis with high efficiency for the signal, while rejecting a large portion of SM backgrounds. A Boosted Decision Tree (BDT) discriminant is trained to discriminate the signal against the dominant backgrounds consisting of top-quark pair ($t\bar{t}$) and Drell-Yan (DY) production. A number of kinematic variables characterising event topology are used in the BDT training. For example, small (large) angular separation between the two b -jets (between the dimuon and the di- b -jets systems) characterises the signal topology at lower m_a , while the opposite is true for higher m_a . The BDT training is done separately at each signal mass in order to maximally exploit mass-dependent signal characteristics and maximise the sensitivity across the considered m_a range. The dimuon invariant mass spectrum is scanned in 2 GeV or 3 GeV wide bins in search for an excess above the background model. The background expectations and the observed data in all the bins are shown in Figure 1. The largest deviation is observed at 52 GeV and corresponds to a local (global) significance of 3.3σ (1.7σ). The upper limits on $B(H \rightarrow aa \rightarrow 2b2\mu)$ are shown in Figure 2, left, in red (observed) and black (expected). The limits are compared to the result from an earlier ATLAS publication based on 36 fb^{-1} of data⁶ (blue lines) and show factors 2–5 improvement over the full mass range.

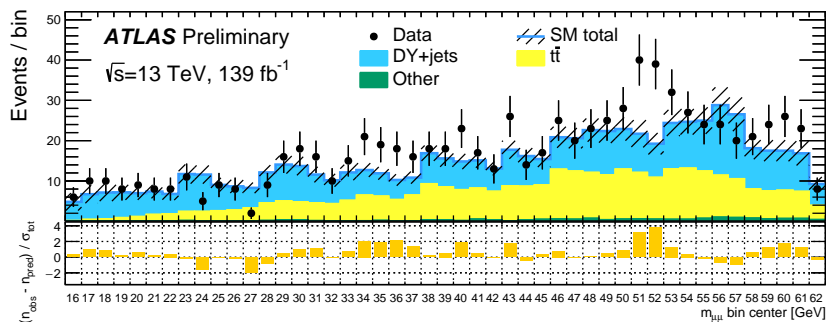


Figure 1 – Observed data and estimated backgrounds in all $m_{\mu\mu}$ bins that are tested for the presence of signal in $H \rightarrow aa \rightarrow 2b2\mu$ analysis⁵. The bins are 2 GeV (3 GeV) wide in $m_{\mu\mu}$ for $m_a \leq 45$ GeV ($m_a > 45$ GeV). Events in neighbouring bins partially overlap. The bottom panel shows the pull in each bin, defined as $(n_{\text{obs}} - n_{\text{pred}}) / \sigma_{\text{tot}}$, where n_{obs} is the number of events in the data, n_{pred} is the number of the fitted background events and σ_{tot} is the total (systematic and statistical, added in quadrature) uncertainty on the fitted background yield.

2.2 $H \rightarrow aa \rightarrow 4b$

The ATLAS search for boosted pseudoscalars in the $15 < m_a < 30$ GeV mass range⁷ developed specialised techniques to tag low-mass $a \rightarrow bb$ objects. The analysis uses lepton triggers to target

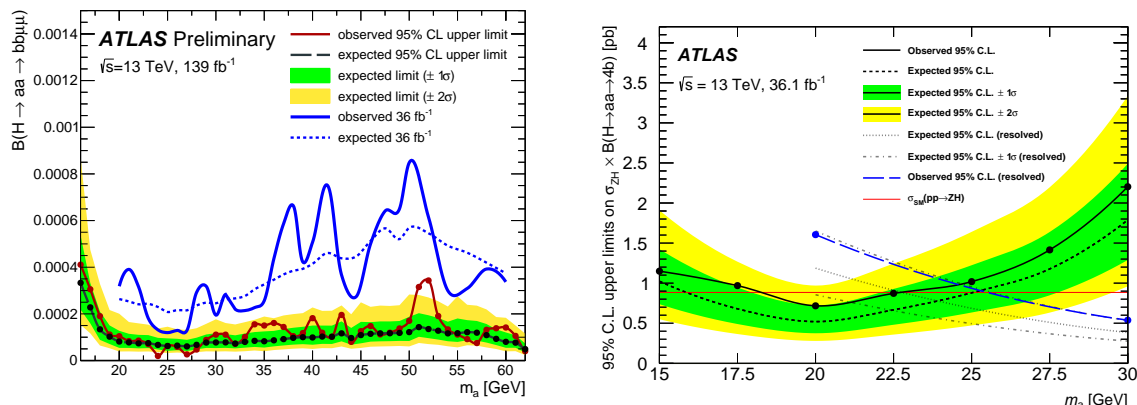


Figure 2 – Upper limits on $B(H \rightarrow aa \rightarrow 2b2\mu)$ obtained with 139 fb^{-1} of data⁵ (left) and $\sigma_{ZH} \times B(H \rightarrow aa \rightarrow 4b)$ obtained with 36.1 fb^{-1} of data⁷ (right) as a function of the signal mass. Black and red dots show masses for which the hypothesis testing was done. Blue lines show comparisons with previously published ATLAS results based on 36 fb^{-1} of data: $H \rightarrow aa \rightarrow 2b2\mu$ search⁶ (left) and $H \rightarrow aa \rightarrow 4b$ search in the final state with four resolved b -jets⁸ (right).

events where the Higgs boson is produced in association with a Z -boson and Z -boson decays leptonically. The $a \rightarrow bb$ reconstruction procedure starts by reclustering jets with the standard radius parameter of $R = 0.4$ into larger $R = 0.8$ jets. Tracks matched to $R = 0.8$ jets are clustered into two or three sub-jets using the Exk_t ⁹ algorithm. With this procedure, b -quarks are associated to different sub-jets with nearly 100% efficiency. A BDT discriminant is trained to distinguish $a \rightarrow bb$ from the background of jets containing only one b -quark. Multivariate b -tagging scores of the sub-jets, the angular separation between the sub-jets and the p_T asymmetry, $(p_T^1 - p_T^2)/(p_T^1 + p_T^2)$, are used in the training. Two working points of the tagger are calibrated in the data using gluon $\rightarrow bb$ events and used to define a set of control and signal regions with different signal versus background contributions and different background compositions. The upper limits on $B(H \rightarrow aa \rightarrow 4b)$ are shown in Figure 2, right. Below $m_a = 25 \text{ GeV}$, there is a significant gain in sensitivity compared to the resolved analysis⁸ shown in blue. At around $m_a = 20 \text{ GeV}$, the boosted analysis is probing the region below $B(H \rightarrow aa \rightarrow 4b) < 100\%$, setting a solid ground for future improvements.

2.3 $H \rightarrow aa \rightarrow 2\mu 2\tau$

CMS searched for $H \rightarrow aa$ in the $3.6 < m_a < 21 \text{ GeV}$ mass range in the final state with two muons ($a \rightarrow \mu\mu$), one hadronically decaying τ and one leptonically (muon) decaying τ , $a \rightarrow \tau_h \tau_\mu$ ¹⁰. In this mass range, the two τ -leptons are collimated and a specialised reconstruction technique is developed in order to reconstruct the $a \rightarrow \tau_h \tau_\mu$ object. Standard hadron-plus-strips (HPS) algorithm¹¹ for reconstruction of τ_h candidates is modified in two ways. Firstly, muons with $p_T > 3 \text{ GeV}$ are removed from jets seeding the HPS algorithm, resulting in a significant increase in $a \rightarrow \tau_h \tau_\mu$ reconstruction efficiency at lower masses (see Figure 3). Secondly, the muon energy is excluded from the τ_h isolation discriminant, resulting in an efficiency increase over the whole mass range. Standard Model backgrounds are constrained in a 2D unbinned fit to the dimuon and four-object ($m_{\mu\mu\tau_h\tau_\mu}$) invariant masses. The background model fits the data well and no significant excess above the SM predictions is observed. The upper limits on $B(H \rightarrow aa \rightarrow 2\mu 2\tau)$ are shown in Figure 3.

2.4 $H \rightarrow aa$ summary plots

Model independent limits on $B(H \rightarrow aa \rightarrow xxyy)$, where x and y represent various final-state particles, are translated into limits on $B(H \rightarrow aa)$ under an assumption of a particular

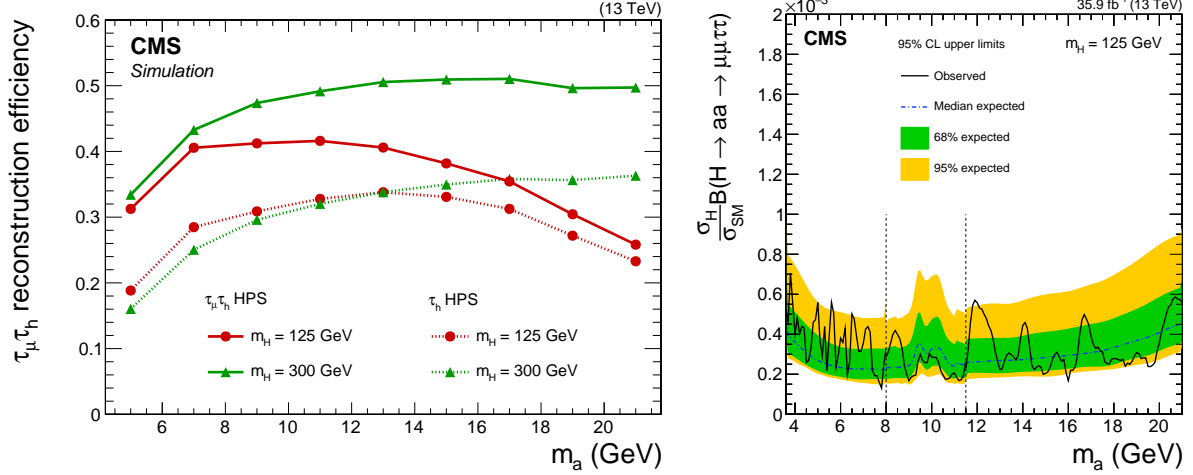


Figure 3 – Left: The efficiency of the standard HPS (dashed lines) and $\tau_h \tau_\mu$ HPS reconstruction used in $H \rightarrow aa \rightarrow 2\mu 2\tau$ analysis¹⁰ (solid lines) as a function of m_a . Right: Upper limits on $\frac{\sigma_H}{\sigma_{SM}} B(H \rightarrow aa \rightarrow 2\mu 2\tau)$ as a function of the signal mass.

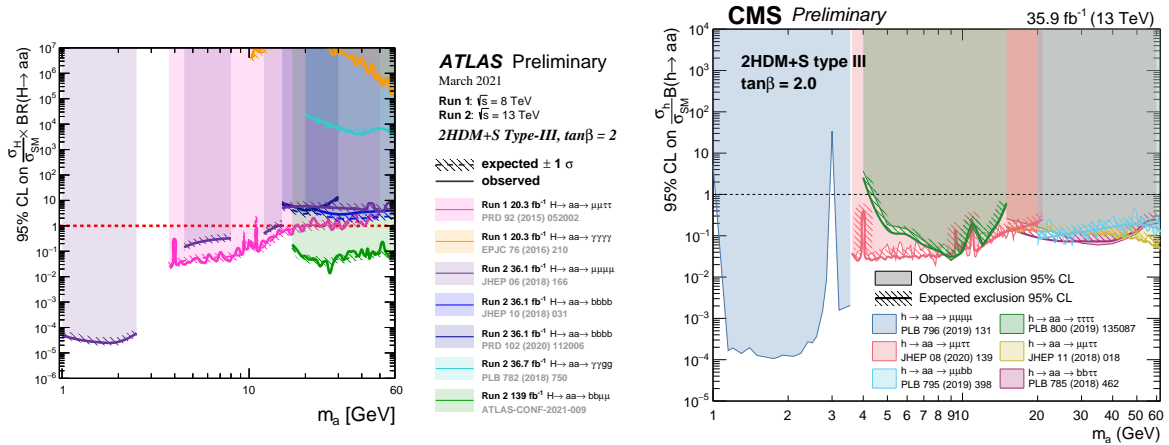


Figure 4 – Overlay of observed and expected upper limits on $\frac{\sigma_H}{\sigma_{SM}} B(H \rightarrow aa)$ in Type-III 2HDM+S scenario with $\tan\beta=2$ for ATLAS¹² (top) and CMS¹³ (bottom).

2HDM+S scenario that specifies $B(aa \rightarrow xyy)$. Figure 4 shows interpretations of ATLAS and CMS $H \rightarrow aa$ searches^{12,13} in the Type-III 2HDM+S scenario^{4,14}, with the ratio of vacuum expectation values of the two Higgs doublets $\tan\beta=2$. The plots demonstrate how different final states dominate the sensitivity at different m_a . In the full mass range the observed limits are below the current upper limit on $B(H \rightarrow \text{undetected})$ of 19%, i.e. direct searches for exotic Higgs decays are probing so far unconstrained phase space.

3 Lepton-flavor violating decays

3.1 $H \rightarrow \mu\tau/e\tau$

Lepton-flavour violating decays of the Higgs boson are searched for by CMS in four channels: $\mu\tau_h$, $\mu\tau_e$, $e\tau_h$ and $e\tau_\mu$ ¹⁵. The standard HPS algorithm is used to reconstruct τ_h . A BDT discriminant is trained in each channel separately. Typical input variables to the training, among others, are lepton transverse momenta, $\Delta\phi$ separation between the leptons and the missing transverse momentum and the transverse mass. Each channel is further divided into four event categories, based on the number of jets in the final state and the di-jet invariant mass, to enhance different Higgs production mechanisms. A simultaneous fit to the BDT distributions is performed over

all channels and categories to extract upper limits on $B(H \rightarrow \mu\tau)$ and $B(H \rightarrow e\tau)$. The result is shown in Figure 5. The upper limits set on $B(H \rightarrow \mu\tau)$ and $B(H \rightarrow e\tau)$ amount to 0.15% and 0.22%, respectively, and improve previous ATLAS and CMS results by about a factor two.

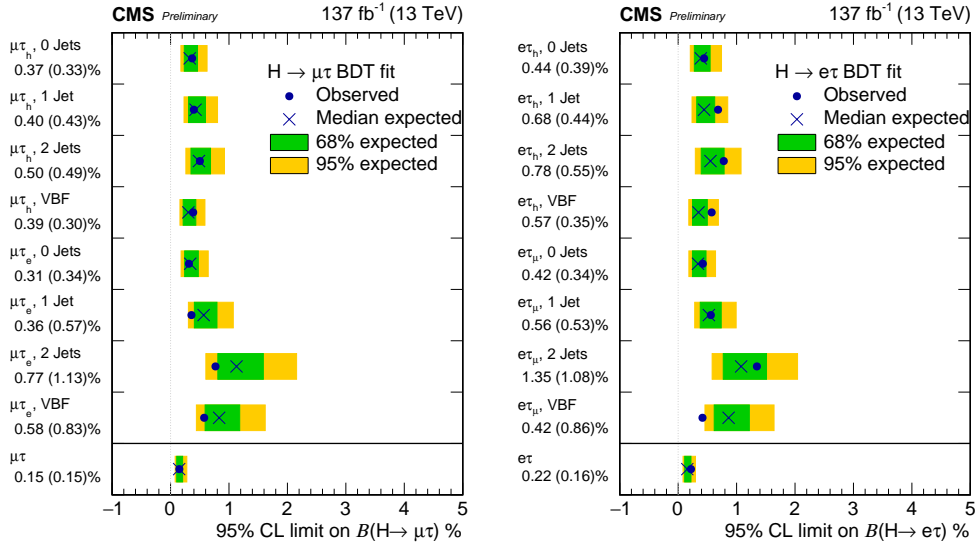


Figure 5 – Observed and expected upper limits on lepton-flavor violating Higgs branching fractions, $B(H \rightarrow \mu\tau)$ (left) and $B(H \rightarrow e\tau)$ (right), shown for each event category separately and for all the categories combined¹⁵.

4 Rare decays

4.1 $H \rightarrow \ell\ell\gamma$

ATLAS searched for the Higgs boson decay into two leptons (muons or electrons) and a photon, in the kinematic range where the dilepton mass, $m_{\ell\ell}$, is below 30 GeV¹⁶. In this mass range, the analysis is mainly sensitive to dilepton production through γ^* . Multiple event categories, such as $ee/\mu\mu$ resolved, ee merged, VBF enhanced, are treated separately to maximise the analysis sensitivity. A dedicated technique to reconstruct merged electrons is developed to improve the efficiency in this category. The $H \rightarrow \ell\ell\gamma$ signal is observed with a significance of 3.2σ , providing a first evidence of this rare Higgs decay. Figure 6 shows the 3-object invariant mass, $m_{\ell\ell\gamma}$, spectrum, with the combined signal-plus-background model fit to all analysis categories simultaneously shown with the red curve. The best-fit value of the signal-strength parameter, defined as the ratio of the observed signal yield to the signal yield expected in SM, is measured to be $\mu = 1.5 \pm 0.5$.

5 Summary

This presentation summarised several recent searches for rare and exotic Higgs boson decays carried out by the ATLAS and CMS collaborations. The presented analyses are based on the data from 13 TeV proton-proton collisions at the LHC. The searches for Higgs boson decays into BSM particles and lepton-flavor violating Higgs decays continue to probe so-far unconstrained parameter space. In the domain of rare Higgs decays, evidence for the rare $H \rightarrow \ell\ell\gamma$ decays was found in ATLAS, amounting to an observed significance of 3.2σ .

References

1. ATLAS Collaboration, ATLAS-CONF-2020-027, <http://cdsweb.cern.ch/record/2725733>.

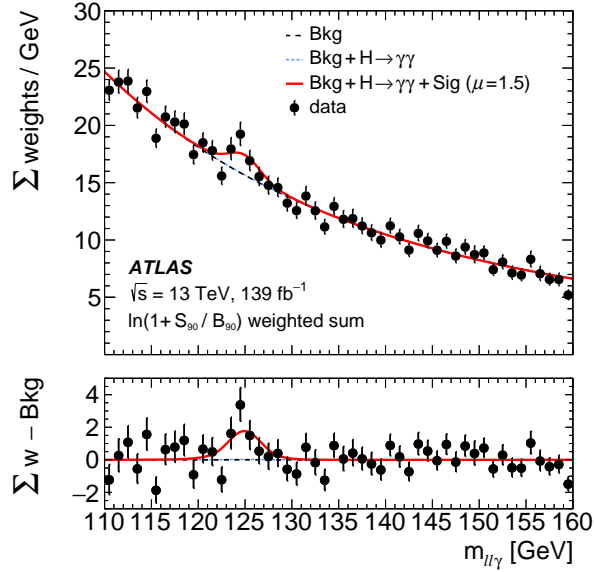


Figure 6 – The $m_{\ell\ell\gamma}$ distribution from all the event categories considered in the $H \rightarrow \ell\ell\gamma$ search¹⁶, added with a category-dependent weight. The red curve shows the combined signal-plus-background model. The bottom panel shows the residuals of the data with respect to the non-resonant background component of the signal-plus-background fit.

2. ATLAS Collaboration, JINST 3 (2008) S08003.
3. CMS Collaboration, JINST 3 (2008) S08004.
4. D. Curtin *et al*, *Phys. Rev. D* **90**, 075004 (2014).
5. ATLAS Collaboration, ATLAS-CONF-2021-009, <http://cdsweb.cern.ch/record/2759283>.
6. ATLAS Collaboration, *Phys. Lett. B* **790**, 1 (2019).
7. ATLAS Collaboration, *Phys. Rev. D* **102**, 112006 (2020).
8. ATLAS Collaboration, JHEP 10 (2018) 031.
9. S. Catani *et al*, Nucl. Phys. B406 (1993) 187.
10. CMS Collaboration, JHEP 08 (2020) 139.
11. CMS Collaboration, JINST 13 (2018) P10005.
12. ATLAS Collaboration, ATLAS-PHYS-PUB-2021-008, <http://cdsweb.cern.ch/record/2758783>.
13. CMS Collaboration, <https://twiki.cern.ch/twiki/bin/view/CMSPublic/Summary2HDMSRun2>.
14. U. Haisch *et al*, arXiv:1802.02156 [hep-ph].
15. CMS Collaboration, CMS-PAS-HIG-20-009, <https://cds.cern.ch/record/2758334>.
16. ATLAS Collaboration, arXiv:2103.10322 [hep-ex].